A Stochastic Geometry Based Techno-Economic Analysis of RIS-Assisted Cellular Networks

Guodong Sun[1,2,3], François Baccelli[1,2], Luis Uzeda Garcia[3], and Stefano Paris[3]

[1]Department d'informatique, Ecole Normale Supérieure. Email: guodong.sun|francois.baccelli@ens.fr
[2]Institut national de recherche en sciences et technologies du numérique (INRIA)
[3]Nokia Networks France. Email: luis.uzeda_garcia|stefano.paris@nokia.com

***Abstract*—Reconfigurable intelligent surfaces (RISs) are a promising technology for enhancing cellular network performance and yielding additional value to network operators. This paper proposes a techno-economic analysis of RIS-assisted cellular networks to guide operators in deciding between deploying additional RISs or base stations (BS). We assume a relative cost model that considers the total cost of ownership (TCO) of deploying additional nodes, either BSs or RISs. We assume a return on investment (RoI) that is proportional to the system's spectral efficiency. The latter is evaluated based on a stochastic geometry model that gives an integral formula for the ergodic rate in cellular networks equipped with RISs. The marginal RoI for any investment strategy is determined by the partial derivative of this integral expression with respect to node densities. We investigate two case studies: throughput enhancement and coverage hole mitigation. These examples demonstrate how operators could determine the optimal investment strategy in scenarios defined by the current densities of BSs and RISs, and their relative costs. Numerical results illustrate the evolution of ergodic rates based on the proposed investment strategy, demonstrating the investment decision-making process while considering technological and economic factors. This work quantitatively demonstrates that strategically investing in RISs can offer better system-level benefits than solely investing in BS densification.**

***Index Terms*—Techno-economic analysis, stochastic geometry, sensitivity analysis, cellular network**

I. Introduction

The reconfigurable intelligent surface (RIS) technology is considered a promising complement to base stations (BS) and is expected to enhance a wide range of wireless services, including extended coverage, higher data rates, and improved reliability [1]. A RIS is composed of numerous low-cost reflectors that can intelligently shape radio signals with minimal power consumption, as only configuration energy is required. This makes the capital expenditure of deploying RIS hardware lower than other beamforming technologies that rely on active antenna arrays [2]. RISs can also reduce networks' operation expenditure since they consume less power compared to BSs [3]. Additionally, since RISs have no power amplification, they generate less interference than BSs, and this feature also contributes to power efficiency and cost savings. Overall, the RIS technology may offer a cost-effective alternative to deploying additional BSs in cellular networks.

While many researchers have addressed the technical challenges of incorporating RISs into cellular networks, few results are available to assess economic questions quantitatively. In the literature on relay technology, the system-level techno-economic analyses mostly relied on Monte Carlo simulation results to quantify the expenditure for different technologies [4]. An analytical approach would be most helpful in quantifying the techno-economic trade-offs associated with RIS deployment.

Stochastic geometry [5] serves as a powerful analytical tool for modeling and evaluating RIS-assisted networks, effectively capturing the inherent uncertainty in user location and irregularity in node placement. For example, the authors in [6] model both BSs and RISs as homogeneous Poisson point processes (PPP) and associate the typical user equipment (UE) to the nearest BS and RIS. By approximating the composite signal with a Gamma distribution, the authors derive a double integral expression to quantify the coverage probability. Recently, the authors in [7] proposed a novel framework that captures the random placement of both BSs and RISs, enabling the performance analysis of a variety of RIS applications, such as throughput enhancement or coverage hole mitigation.

In this work, we address the analysis of RISs from a techno-economic perspective using the stochastic geometry tools developed in [7] to characterize the ergodic rate of a typical UE, which reflects the spectral efficiency at the system level. To assess the marginal spectral efficiency of an investment, we introduce a new sensitivity analysis step into the integral expressions obtained in [7]. One of our contributions is the verification of conditions for interchanging integration and differentiation operations. More precisely, the present paper provides integral formulas to compute the partial derivatives of the ergodic rate of a typical UE with respect to (w.r.t.) the density of BSs and that of RISs. By applying these formulas to a given cellular network with RISs, we can quantify the expected gain from increasing BS or RIS densities. This could be used to guide operators in deciding whether to invest in additional BSs or RISs so as to optimize the total cost of ownership (TCO). This investment strategy requires knowledge of the current densities of BSs and RISs and their relative costs, assuming a simplified return on investment (RoI) proportional to the ergodic rate of a typical UE[1].

[1]A higher ergodic rate generally correlates with an increased RoI, though various economic factors influence the exact relationship. A direct proportionality serves as a useful initial estimate.

ISBN 978-3-903176-73-7 © 2025 IFIP

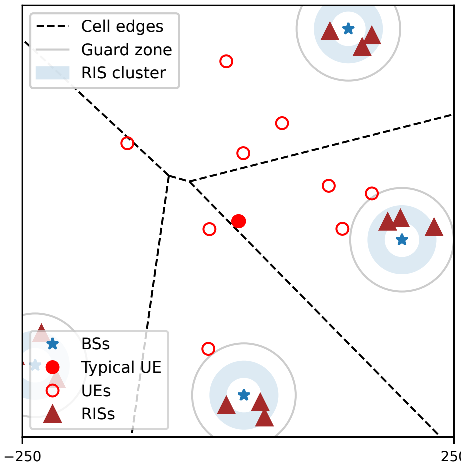

Fig. 1: Modeling RIS-assisted Cellular Networks with Matérn Cluster Processes, with a guard zone to prevent the typical UE from being near BSs or RISs.

This work is organized as follows: we present the system model of the RIS-assisted cellular network and discuss the TCO estimation in Section II. We derive the first-order derivative expressions of the system performance w.r.t. the densities of BSs and RISs, and discuss the optimal investment strategy in Section III. Numerical results are presented in Section IV, where we interpret the techno-economic analysis. We conclude this paper in Section V.

II. Stochastic Geometry System Model

RISs can be deployed to address two primary use cases: enhancing network throughput and mitigating coverage holes. We present the stochastic geometry models of these two scenarios, accounting for the randomness of wireless network deployments. We also model the TCO for deploying BSs or RISs per unit area.

A. Thoughput Enhancement Model

We investigate the throughput enhancement scenario by modeling BSs and RISs as Matérn cluster processes (MCP), where RISs are clustered around the BSs to serve the UEs in the cell, depicted in Fig. 1. The location of BSs is modeled as a homogeneous PPP $\Phi_{\mathrm{BS}} \triangleq \sum_{i\in\mathcal{I}} \delta_{\mathbf{x}_i}$ with intensity λ_{BS}, where δ denotes the Dirac delta function, modeling the mother process of the MCP. Here, $\mathcal{I}$ is the index set of BSs. Each RIS is assumed to be associated with a serving BS and the placement of RISs is modeled as the daughter processes of the MCP $\Phi_{\mathrm{RIS}} = \cup_{i\in\mathcal{I}}\phi_i$, where ϕ_i denotes the RIS cluster of BS i. By definition, $\phi_i = \sum_{j\in\mathcal{J}_i} \delta_{\mathbf{y}_{i,j}}$, where $\mathcal{J}_i$ is the index set of RISs of cluster i, is a PPP with intensity λ_{RIS}, with support on the ring $\mathbb{D}_{\mathbf{x}_i}(R_{\mathrm{in}}, R_{\mathrm{out}})$ of center $\mathbf{x}_i$, inner radius R_{in} and outer radius R_{out}. In addition, the UE locations are modeled as a homogeneous PPP Φ_{UE} with intensity λ_{UE}, which is independent of Φ_{BS} and Φ_{RIS}. We consider a guard zone to exclude UEs near BSs from throughput enhancement evaluation, as strong signals experienced by these UEs reduce the need for RIS configuration and overhead. Therefore, we only consider UEs beyond a certain distance R_c to be jointly served by the BS and RISs in this cell, as indicated by the gray contour in Fig. 1. The typical UE in Φ_{UE}, marked as the filled red circle, is located at the origin o and is served by its closest BS and the associated RIS cluster that is specifically indexed by o. The probability distribution function (PDF) of the distance from the serving BS to the typical UE is $f(r) = 2\pi\lambda_{\mathrm{BS}} r e^{-\lambda_{\mathrm{BS}}\pi r^2}$ [8][9], with $r \triangleq ||\mathbf{x}_o||$.

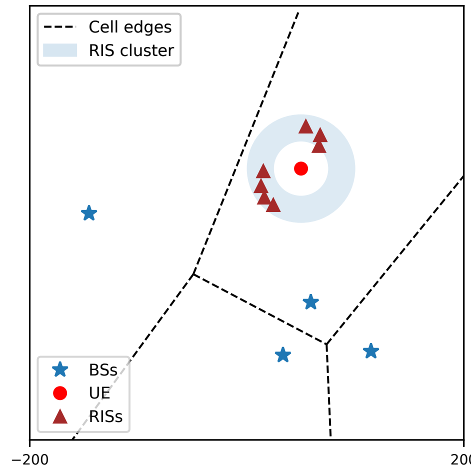

Fig. 2: RISs are deployed to assist UEs in coverage holes

B. Coverage Hole Mitigation Model

To investigate coverage hole mitigation, we consider a scenario where a UE located at the center of a coverage hole experiences signal attenuation on the direct link. We consider a cluster of RISs $\mathcal{J}_o$ is deployed in a ring around this hole, as shown in Fig. 2. To model the effect of blockage on signal attenuation, we assume the direct link from the BS to the UE is penalized by a constant attenuation coefficient K. To model the distance between the coverage hole and the associated BS, we remark that the spatial distribution of BSs will impact the proximity of an arbitrary location to its closest BS [10]. For the two-dimensional PPP-modeled BSs, the expected value of this distance is inversely proportional to the square root of λ_{BS}. In this work, we consider an average scenario where the centers of both the coverage hole and the RIS ring are located at a distance r_{H} from its associated BS, which is a function of the BS density, given by

$$r_{\mathrm{H}} = \frac{C_{\mathrm{H}}}{\sqrt{\lambda_{\mathrm{BS}}}}, \tag{1}$$

where C_{H} is a constant, whose value is selected in the simulation section ensuring that the coverage hole and the cluster of RISs are with high probability within the cell.

Without loss of generality, we assume that the RISs can effectively serve their associated UEs[2]. In other words, each RIS is modeled as a point and is capable of reflecting signals in any direction according to a given RIS-UE association. Note that both models contain the special case of the scenario without deploying RISs by setting $\lambda_{\mathrm{RIS}} = 0$.

[2]Models of reflective, refractive, or hybrid (reflective and refractive) RISs can be analyzed using the same method by changing the density of the corresponding RIS type.

C. System Performance Analysis

The channel from the BS to the UEs assisted by multiple RISs is time-dispersive. This is because the RISs are spatially dispersed and the propagation distance of the direct and reflected paths are different. It is shown in [7] that employing orthogonal frequency-division multiplexing (OFDM) modulation to mitigate the time-dispersion of the channel caused by multipath reflections, the post-processed signal-to-interference-plus-noise ratio (SINR) is given by

$$\mathrm{SINR} = \frac{|\gamma_{D_o}|^2 + \sum_{j\in\mathcal{J}_o}|\gamma_{R_{o,j}}|^2}{\sum_{i\in\mathcal{I}\setminus o}(|\gamma_{D_i}|^2 + \sum_{j\in\mathcal{J}_i}|\gamma_{R_{i,j}}|^2) + \sigma^2}, \quad (2)$$

where σ^2 is the power of the additive Gaussian noise. Here, γ_{D_o} and $\gamma_{R_{o,j}}$ represent the received signal amplitude of the direct and reflected intended signals, respectively, while γ_{D_i} and $\gamma_{R_{i,j}}$ represent the corresponding received signal amplitude of the direct and reflected interference, respectively. Each signal amplitude is typically the product of a fading variable $\rho \in \mathbb{C}$, a transmission power P_0, and a pathloss function as the function of propagation distance. Specifically, the direct pathloss is given by $\gamma_D = \rho\sqrt{g(d)P_0}$ for distance d while the reflected pathloss is $\gamma_R = \rho\sqrt{g(d_1)g(d_2)P_0}$, where the latter accounts for the two segments of the reflected path. Below, we take $g(d) = \beta(d+1)^{-\alpha}$, where the pathloss exponent $\alpha > 2$, and where $\beta = \frac{c}{4\pi f_c}$ is the average power gain for reference distance of 1m, f_c is the carrier frequency, and c denotes the speed of light.

The direct links are assumed to experience a Rayleigh fading $\rho_D \in \mathbb{C}$. As for the reflected links, the fading experienced by one RIS element, denoted by ζ, is computed as the product $\rho_{\mathrm{BS-RIS}} \cdot \rho_{\mathrm{RIS-UE}}$ of two small-scale fading coefficients. This is because each RIS element is modeled as a lossless phase shifter that can scatter the absorbed energy with a proper phase shift [11], [12]. Both $\rho_{\mathrm{BS-RIS}}$ and $\rho_{\mathrm{RIS-UE}}$ are assumed to follow a Rician distribution due to line-of-sight channel conditions, as RISs are usually deployed in favorable locations. The small-scale fading of a reflected beam, formed by phase alignment of M elements of a RIS panel, can be approximated by a Gaussian distributed random variable. This approximation relies on the central limit theorem, since the reflected beam magnitude is the sum of fading amplitude from a large number of RIS elements, given by $|\rho_R| = \sum_{m=1}^{M}|\zeta^{(m)}| \approx \mathcal{N}(M\mathbb{E}[|\zeta|], M\mathbb{V}[|\zeta|])$, where $|\zeta^{(m)}|$ is the fading for the m^{th} element. Consequently, the power of the fading of a reflected beam follows the non-central chi-square distribution, denoted by $|\rho_R|^2 \sim \chi^2$.

D. Total Cost of Ownership

Below, we model the TCO by considering two cost categories for both BS and RIS, namely, the capital expenditure (CAPEX) and the operational expenditure (OPEX). These are denoted by $C_{\mathrm{BS}}, C_{\mathrm{RIS}}$ and $O_{\mathrm{BS}}, O_{\mathrm{RIS}}$, respectively.

From the observation that RIS is cost-effective compared to BS, which employs full radio-frequency (RF) chains [2], we assume that the total CAPEX are such that $C_{\mathrm{BS}} > C_{\mathrm{RIS}}$. Leveraging the fact that a given RIS is expected to require less power and maintenance [13], we also assume that the total OPEX satisfy $O_{\mathrm{BS}} > O_{\mathrm{RIS}}$. The TCO is $\bar{C}_{\mathrm{BS}} = O_{\mathrm{BS}} + C_{\mathrm{BS}}$ for each BS and $\bar{C}_{\mathrm{RIS}} = O_{\mathrm{RIS}} + C_{\mathrm{RIS}}$ for each RIS. Next, we introduce the parameter defining the cost ratio $J = \bar{C}_{\mathrm{BS}}/\bar{C}_{\mathrm{RIS}}$, which will be used in the techno-economic analysis.

Note that the λ_{RIS} represents the density of RISs within each cluster, which is conditioned on the spatial distribution of BSs. When evaluating an investment policy for performance enhancement, the cost of deploying additional network elements, whether BSs or RISs, depends on the total number of elements added to an area. To achieve a fair comparison of deployment costs, the area-dependent cost, $\Delta\bar{C}_{\mathrm{RIS}}$, for increasing the RIS density, $\Delta\lambda_{\mathrm{RIS}}$, should be normalized in terms of the total area allocated for RIS deployment, rather than in terms of the cluster area of each cell. The normalized cost is given by

$$\Delta\bar{C}_{\mathrm{RIS}} = \bar{C}_{\mathrm{RIS}}\lambda_{\mathrm{BS}}\mathcal{A}\Delta\lambda_{\mathrm{RIS}}, \quad (3)$$

where $\mathcal{A}$ denotes the area of a cluster ring and $\lambda_{\mathrm{BS}}\mathcal{A}$ represents the total area of RIS cluster per unit area. Furthermore, when each BS is assumed to associate with $\mathcal{A}\lambda_{\mathrm{RIS}}$ RISs, increasing the BS density $\Delta\lambda_{\mathrm{BS}}$ implies adding the associated RISs, resulting in the cost $\Delta\bar{C}_{\mathrm{BS}}$ due to both BSs and RISs, given by

$$\Delta\bar{C}_{\mathrm{BS}} = \bar{C}_{\mathrm{BS}}\Delta\lambda_{\mathrm{BS}} + \bar{C}_{\mathrm{RIS}}\mathcal{A}\lambda_{\mathrm{RIS}}\Delta\lambda_{\mathrm{BS}}. \quad (4)$$

III. Sensitivity Analysis and Investment Strategy

In this section, we quantify the ergodic rate improvement of the UE, located either in a throughput-enhanced area or at the center of a coverage hole, as a function of increasing either the BS density or the RIS density. In addition, we propose an incremental deployment strategy to assist network operators in making informed decisions about BS and RIS investments.

A. Integral Expression for Mean Ergodic Rate

Reflected interference from RISs in non-associated cells, denoted by $\sum_{j\in\mathcal{J}_i}|\gamma_{R_{i,j}}|^2$ for all $i \neq o$, can be negligible under certain conditions. Specifically, when non-associated reflected beams from other cells are randomly directed and have a low probability of overlapping with the UE of interest, the impact of this interference is minimal, as shown in [7]. We will empirically verify this condition in the simulation section. Assuming this factor has negligible influence on investment decision-making, we will neglect it in the following analysis.

A communication link is considered successfully covered when $\mathrm{SINR} \geq T$, where T is the coverage threshold. The coverage probability is then defined as $\mathsf{P}(T) \triangleq \mathbb{P}[\mathrm{SINR} \geq T]$. By manipulating SINR in Eq. (2) with T, we have

$$|\gamma_{D_o}|^2 \geq T\Big(\sum_{i\in\mathcal{I}\setminus o}|\gamma_{D_i}|^2 + \sigma^2\Big) - \sum_{j\in\mathcal{J}_o}|\gamma_{R_{o,j}}|^2, \quad (5)$$

where $I = \sum_{i\in\mathcal{I}\setminus o}|\gamma_{D_i}|^2$ represents the total power of the aggregated interference and $S_R = \sum_{j\in\mathcal{J}_o}|\gamma_{R_{o,j}}|^2$ the total power of the reflected signals, respectively. Denote the right-hand side of Eq. (5) by $\Upsilon \in \mathbb{R}$ as a function of the threshold T. The Laplace transform of Υ can be expressed as the product of the Laplace transform of the scaled interference power I, the noise power σ^2, and the reflected signals power $-S_R$, since they are built from independent random point processes and random variables, given by[3] $\mathcal{B}_\Upsilon(s) = \mathcal{B}_I(sT)\mathcal{B}_{\sigma^2}(sT)\mathcal{B}_{-S_R}(s)$. Specifically, $\mathcal{B}_I(sT)$ is obtained from the probability generating functional (PGFL) of the PPP, given by

$$\mathcal{B}_I(sT) = e^{-2\pi\lambda_{\mathrm{BS}}\int_r^\infty x\left(1-\mathcal{L}_{|\rho_D|^2}(sTP_0 g(x))\right)\mathrm{d}x}, \tag{6}$$

where the Laplace transform of the Rayleigh faded interfering signal is $\mathcal{L}_{|\rho_D|^2}\big(sTP_0 g(x)\big) = \frac{1}{1+sTP_0 g(x)}$. In addition, for the Gaussian noise, we have $\mathcal{B}_{\sigma^2}(sT) = e^{-sT\sigma^2}$. Similarly, the Laplace transform for the reflected signals is built from the PPP of the RIS cluster associated with the typical BS:

$$\mathcal{B}_{-S_R}(s) = e^{-\lambda_{\mathrm{RIS}}\int_{R_{\mathrm{in}}}^{R_{\mathrm{out}}}\int_0^{2\pi} y\left(1-\mathcal{L}_{|\rho_R|^2}(-sP_0 G(r,y,\psi))\right)\mathrm{d}\psi\mathrm{d}y}. \tag{7}$$

Here, the pathloss of the reflected path is $G(r,y,\psi) = g(y)g(\sqrt{r^2+y^2-2ry\cos\psi})$, where $r = \|\mathbf{x}_o\|, y = \|\mathbf{y}\|$, represent the distances of the BS and RIS to the UE, respectively, and $\psi \in [0, 2\pi)$ is the angle between the two segments of the reflected link. In addition, the Laplace transform of the fading power of the reflected beam $|\rho_R|^2 \sim \chi^2$ is given by

$$\mathcal{L}_{|\rho_R|^2}(s) = \frac{\exp\left(\frac{-s(M\mathbb{E}[|\zeta|])^2}{1+2sM\mathbb{V}[|\zeta|]}\right)}{(1+2sM\mathbb{V}[|\zeta|])^{1/2}}, \tag{8}$$

where $s > -\frac{1}{2M\mathbb{V}[|\zeta|]}$ specifies the region of convergence of the Laplace transform expression.

We can now state the integral representation of the coverage probability [7, Theorem 1]:

Theorem 1. *The coverage probability for a typical UE located at a distance of r to the associated BS is given by*

$$\mathsf{P}_c(T|r) = \mathcal{B}_{\Upsilon^+}\left(\frac{1}{P_0 g(r)}\right), \tag{9}$$

where $\mathcal{B}_{\Upsilon^+}(s)$ is given by the singular integral

$$\mathcal{B}_{\Upsilon^+}(s) = \frac{1}{2\pi\imath}\int_{-\infty}^{\infty}\Big(\mathcal{B}_\Upsilon(s-\imath u)-\mathcal{B}_\Upsilon(-\imath u)\Big)\frac{\mathrm{d}u}{u}+\frac{1+\mathcal{B}_\Upsilon(s)}{2}, \tag{10}$$

where $\imath$ is the imaginary unit. $\int_{-\infty}^{\infty}\frac{\mathrm{d}u}{u}$ is understood in the sense of Cauchy principal-value, $\int_{-\infty}^{\infty} = \lim_{\epsilon\downarrow 0^+}\int_{-\infty}^{-\epsilon}+\int_{\epsilon}^{\infty}$.

Based on the Shannon rate formula and the coverage probability, the mean ergodic rate of a typical UE at a distance r from the associated BS is given by an integral:

$$\tau(r) = \int_0^\infty \mathcal{B}_{\Upsilon^+}\left(\frac{1}{P_0 g(r)}\right)\frac{1}{1+t}\mathrm{d}t. \tag{11}$$

B. Sensitivity Analysis for Throughput Enhancement

To quantify the throughput of RIS-assisted networks, we consider the mean ergodic rate of a UE located at the distance $r \in [R_c, \infty)$ from the BS, given by

$$\tau = \int_0^\infty\int_{R_c}^\infty \mathcal{B}_{\Upsilon^+}\left(\frac{1}{P_0 g(r)}\right)\frac{1}{1+t}2\pi\lambda_{\mathrm{BS}} r e^{-\pi r^2\lambda_{\mathrm{BS}}}\mathrm{d}r\mathrm{d}t, \tag{12}$$

with $\tau(r)$ given in Eq. (11). In what follows, we assume that RoI is proportional to the mean ergodic rate and we represent the differential RoI by partial derivatives. We will then analyze the investment strategy in Subsection III-D.

We now derive the first-order derivatives of Eq. (12) w.r.t. the density of BSs or RISs, while keeping all other variables fixed, which is the basis for economic analysis. Differentiating Eq. (12) requires an interchange of the integration and differentiation operators. For this purpose, an appropriate extension of the Leibniz integral rule [14] is given in Appendix A in [15][4]. Applying the Leibniz integral rule, we get

$$\frac{\partial\tau}{\partial\lambda_{\mathrm{BS}}} = \int_0^\infty\int_{R_c}^\infty\left(\frac{\partial\mathcal{B}_{\Upsilon^+}(s)}{\partial\lambda_{\mathrm{BS}}}\lambda_{\mathrm{BS}}+\mathcal{B}_{\Upsilon^+}(s)(1-\pi r^2\lambda_{\mathrm{BS}})\right) 2\pi r e^{-\pi r^2\lambda_{\mathrm{BS}}}\frac{1}{t+1}\mathrm{d}r\mathrm{d}t. \tag{13}$$

Here, we determine $\frac{\partial\mathcal{B}_{\Upsilon^+}(s)}{\partial\lambda_{\mathrm{BS}}}$ through another application of the Leibniz integral rule to Eq. (10), which also involves interchanging of integration and differentiation. While the Leibniz integral rule requires the function under the integral sign and its derivative to be continuous, the singular integral in Eq. (10) has a singularity at zero and at limit points at infinity. The conditions of this interchange are verified in Appendix A in [15]. Subsequently, we have

$$\frac{\partial\mathcal{B}_{\Upsilon^+}(s)}{\partial\lambda_{\mathrm{BS}}} = \frac{1}{2\pi\imath}\int_{-\infty}^{\infty}\left(\frac{\partial\mathcal{B}_\Upsilon(s-\imath u)}{\partial\lambda_{\mathrm{BS}}}-\frac{\partial\mathcal{B}_\Upsilon(-\imath u)}{\partial\lambda_{\mathrm{BS}}}\right)\frac{\mathrm{d}u}{u}+\frac{1}{2}\frac{\partial\mathcal{B}_\Upsilon(s)}{\partial\lambda_{\mathrm{BS}}}, \tag{14}$$

where the expression for the derivative of the Laplace transform $\mathcal{B}_\Upsilon(s)$ w.r.t. the BS density is given by

$$\frac{\partial\mathcal{B}_\Upsilon(s)}{\partial\lambda_{\mathrm{BS}}} = -\mathcal{B}_\Upsilon(s)\cdot 2\pi\int_r^\infty x\Big(1-\mathcal{L}_{|\rho_D|^2}\big(sTP_0 g(x)\big)\Big)\mathrm{d}x. \tag{15}$$

Similar to Eq. (13), we can derive the following expression for the partial derivative of τ w.r.t. λ_{RIS}, given by

$$\frac{\partial\tau}{\partial\lambda_{\mathrm{RIS}}} = \int_0^\infty\int_{R_c}^\infty\left(\frac{\partial\mathcal{B}_{\Upsilon^+}(s)}{\partial\lambda_{\mathrm{RIS}}}\right)2\pi r\lambda_{\mathrm{BS}} e^{-\pi r^2\lambda_{\mathrm{BS}}}\frac{1}{t+1}\mathrm{d}r\mathrm{d}t, \tag{16}$$

where $\frac{\partial\mathcal{B}_{\Upsilon^+}(s)}{\partial\lambda_{\mathrm{RIS}}}$ can be expressed following the steps in Eq. (14) and Eq. (15).

C. Sensitivity Analysis for Coverage Hole Mitigation

To analyze the impact of RIS on coverage hole mitigation, we are interested in the performance in terms of the ergodic rate of the UE located in the center of the coverage hole. In this case, assuming a fixed BS-UE distance r_{H} eliminates the need for integration over the distance r. Consequently, τ is given by Eq. (11) instead of Eq. (12). Moreover, the derivatives obtained in the previous subsection require further modifications.

Recall that we introduce a penalty factor of K to account for the impact of blocked direct links. This penalty factor influences the argument of the Laplace transform to express the coverage probability in Eq. (9), which is then modified to $\frac{1}{KP_0 g(r_{\mathrm{H}})}$. Furthermore, changing the BS density also varies

[3]We let $\mathcal{B}(s)$ denote bilateral Laplace transform and $\mathcal{L}(s)$ denote unilateral Laplace transform.

[4]This technical report contains supplementary mathematical proofs in the Appendix to verify the conditions of applying the Leibniz rule.

the average distance r_{H} between coverage hole centers and their cell centers, as defined in Eq. (1). In the following, we must consider two factors due to the dependence of r_{H} on λ_{BS}. First, the non-associated BSs within a distance of $[r_{\mathrm{H}}, \infty)$ that generate interference can be closer to the UE for larger values of λ_{BS}. Second, the argument $s = \frac{1}{KP_0 g(r_{\mathrm{H}})}$ is a function of r_{H} and consequently depends on λ_{BS}. Let $f_s(r_{\mathrm{H}}) = \frac{1}{KP_0 g(r_{\mathrm{H}})}$ be the function describing this dependence in the following. The changing rates of these two factors are given by

$$\frac{\partial r_{\mathrm{H}}}{\partial \lambda_{\mathrm{BS}}} = -\frac{C_{\mathrm{H}}}{2\sqrt{\lambda_{\mathrm{BS}}^3}}, \ \frac{\partial f_s(r_{\mathrm{H}})}{\partial \lambda_{\mathrm{BS}}} = -\frac{1}{KP_0 g^2(r_{\mathrm{H}})} \frac{\partial g(r_{\mathrm{H}})}{\partial r_{\mathrm{H}}} \frac{\partial r_{\mathrm{H}}}{\partial \lambda_{\mathrm{BS}}}. \tag{17}$$

Recall that $\mathcal{B}_\Upsilon(s) = \mathcal{B}_I(sT)\mathcal{B}_{-S_R}(s)\mathcal{B}_{\sigma^2}(sT)$, we have

$$\begin{aligned}\frac{\partial \mathcal{B}_\Upsilon(s)}{\partial \lambda_{\mathrm{BS}}} =& \frac{\partial \mathcal{B}_I(sT)}{\partial \lambda_{\mathrm{BS}}} \mathcal{B}_{-S_R}(s)\mathcal{B}_{\sigma^2}(sT) + \frac{\partial \mathcal{B}_{-S_R}(s)}{\partial \lambda_{\mathrm{BS}}} \mathcal{B}_I(sT) \\ & \mathcal{B}_{\sigma^2}(sT) + \frac{\partial \mathcal{B}_{\sigma^2}(sT)}{\partial \lambda_{\mathrm{BS}}} \mathcal{B}_I(sT)\mathcal{B}_{-S_R}(s).\end{aligned} \tag{18}$$

We will discuss the derivatives in Eq. (18) separately. First, for the derivative related to the interference I, we have

$$\frac{\partial \mathcal{B}_I(sT)}{\partial \lambda_{\mathrm{BS}}} = \mathcal{B}_I(sT)\bigg(\mathcal{D}_{\mathrm{BS}}(sT) + \lambda_{\mathrm{BS}} \frac{\partial \mathcal{D}_{\mathrm{BS}}(sT)}{\partial \lambda_{\mathrm{BS}}}\bigg), \tag{19}$$

where $\mathcal{D}_{\mathrm{BS}}(sT) = -2\pi \int_{r_{\mathrm{H}}}^{\infty} \frac{xsTP_0 g(x)}{1+sTP_0 g(x)} \mathrm{d}x$ from Eq. (6). In Eq. (19), the expressions of $\frac{\partial \mathcal{D}_{\mathrm{BS}}(sT)}{\partial \lambda_{\mathrm{BS}}}$ are different when differentiating $\mathcal{B}_\Upsilon(s - \imath u)$ and $\mathcal{B}_\Upsilon(-\imath u)$ in Eq. (10), respectively, For the former, both r_{H} and s are dependent on λ_{BS}. To differentiate $\mathcal{D}_{\mathrm{BS}}(sT)$ w.r.t. λ_{BS}, another application of the Leibniz rule is needed. The condition for this application is discussed in Appendix B in [15]. As a result, $\frac{\partial \mathcal{D}_{\mathrm{BS}}(sT)}{\partial \lambda_{\mathrm{BS}}}$ is given by

$$\begin{aligned}\frac{\partial \mathcal{D}_{\mathrm{BS}}(sT)}{\partial \lambda_{\mathrm{BS}}} =& 2\pi \frac{r_{\mathrm{H}} sTP_0 g(r_{\mathrm{H}})}{1+sTP_0 g(r_{\mathrm{H}})} \frac{\partial r_{\mathrm{H}}}{\partial \lambda_{\mathrm{BS}}} \\ & - \int_{r_{\mathrm{H}}}^{\infty} \frac{2\pi x TP_0 g(x)}{\big(1+sTP_0 g(x)\big)^2} \frac{\partial f_s(r_{\mathrm{H}})}{\partial \lambda_{\mathrm{BS}}} \mathrm{d}x,\end{aligned} \tag{20}$$

where $\frac{\partial r_{\mathrm{H}}}{\partial \lambda_{\mathrm{BS}}}$ and $\frac{\partial f_s(r_{\mathrm{H}})}{\partial \lambda_{\mathrm{BS}}}$ are given in Eq. (17). For the latter, $\mathcal{B}_\Upsilon(-\imath u)$, where the argument $-\imath u$ does not depend on r_{H}, the derivative $\frac{\partial \mathcal{D}_{\mathrm{BS}}(sT)}{\partial \lambda_{\mathrm{BS}}}$ only contains the first part of Eq. (20) since $\frac{\partial f_s(r_{\mathrm{H}})}{\partial \lambda_{\mathrm{BS}}}$ in the second term is equal to zero.

Next, we express the derivative of $\mathcal{B}_{-S_R}(s)$ as

$$\frac{\partial \mathcal{B}_{-S_R}(s)}{\partial \lambda_{\mathrm{BS}}} = \mathcal{B}_{-S_R}(s)\lambda_{\mathrm{RIS}} \frac{\partial \mathcal{D}_{\mathrm{RIS}}(s)}{\partial \lambda_{\mathrm{BS}}}, \tag{21}$$

where we use $\mathcal{D}_{\mathrm{RIS}}(s)$ to abbreviate the exponent without λ_{RIS}, given by

$$-\int_0^{2\pi} \int_{R_{\mathrm{in}}}^{R_{\mathrm{out}}} y\Big(1 - \mathcal{L}_{|\rho_R|^2}\big(-sP_0 G(r_{\mathrm{H}}, y, \psi)\big)\Big) \mathrm{d}y \mathrm{d}\psi.$$

Note that $\frac{\partial \mathcal{D}_{\mathrm{RIS}}(s)}{\partial \lambda_{\mathrm{BS}}}$ necessitates the application of the Leibniz rule to interchange differentiation and integration, given by

$$\begin{aligned}& -\frac{\partial}{\partial \lambda_{\mathrm{BS}}} \int_0^{2\pi} \int_{R_{\mathrm{in}}}^{R_{\mathrm{out}}} y\Big(1 - \mathcal{L}_{|\rho_R|^2}\big(-sP_0 G(r_{\mathrm{H}}, y, \psi)\big)\Big) \mathrm{d}y \mathrm{d}\psi \\ & = \int_0^{2\pi} \int_{R_{\mathrm{in}}}^{R_{\mathrm{out}}} \bigg(y \frac{\partial \mathcal{L}_{|\rho_R|^2}\big(-sP_0 G(r_{\mathrm{H}}, y, \psi)\big)}{\partial \lambda_{\mathrm{BS}}}\bigg) \mathrm{d}y \mathrm{d}\psi,\end{aligned} \tag{22}$$

where the condition is discussed in Appendix B in [15]. When differentiating $\mathcal{L}_{|\rho_R|^2}(-sP_0 G(r_{\mathrm{H}}, y, \psi))$ to obtain the derivatives of $\mathcal{B}_\Upsilon(s - \imath u)$ and $\mathcal{B}_\Upsilon(-\imath u)$ in Eq. (10), we note that in the former, both $G(r_{\mathrm{H}}, y, \psi)$ and s are dependent on r_{H}, whereas in the latter only $G(r_{\mathrm{H}}, y, \psi)$ depends on r_{H}. Consequently, for differentiating $\mathcal{B}_\Upsilon(s - \imath u)$, we have

$$\begin{aligned}& \frac{\partial \mathcal{L}_{|\rho_R|^2}\big(-sP_0 G(r_{\mathrm{H}}, y, \psi)\big)}{\partial \lambda_{\mathrm{BS}}} = \\ & \left(\frac{M(\mathbb{E}[|\zeta|])^2/\mathbb{V}[|\zeta|] - 2sP_0 M\mathbb{V}[|\zeta|]G(r_{\mathrm{H}}, y, \psi) + 1}{(1 - 2sP_0 G(r_{\mathrm{H}}, y, \psi)M\mathbb{V}[|\zeta|])^{5/2}}\right) \\ & P_0 M\mathbb{V}[|\zeta|] \exp\left(\frac{sP_0 G(r_{\mathrm{H}}, y, \psi)(M\mathbb{E}[|\zeta|])^2}{1 - 2sP_0 G(r, y, \psi))M\mathbb{V}[|\zeta|]}\right) \\ & \left(s\frac{\partial G(r_{\mathrm{H}}, y, \psi)}{\partial \lambda_{\mathrm{BS}}} + G(r_{\mathrm{H}}, y, \psi)\frac{\partial f_s(r_{\mathrm{H}})}{\partial \lambda_{\mathrm{BS}}}\right),\end{aligned} \tag{23}$$

where $\frac{\partial G(r_{\mathrm{H}}, y, \psi)}{\partial \lambda_{\mathrm{BS}}} = \frac{\partial G(r, y, \psi)}{\partial r_{\mathrm{H}}} \cdot \frac{\partial r_{\mathrm{H}}}{\partial \lambda_{\mathrm{BS}}}$, with $\frac{\partial r_{\mathrm{H}}}{\partial \lambda_{\mathrm{BS}}}$ and $\frac{\partial f_s(r_{\mathrm{H}})}{\partial \lambda_{\mathrm{BS}}}$ given in Eq. (17). For differentiating $\mathcal{B}_\Upsilon(-\imath u)$, where the argument $-\imath u$ does not depend on r_{H}, the factor $G(r_{\mathrm{H}}, y, \psi)\frac{\partial f_s(r_{\mathrm{H}})}{\partial \lambda_{\mathrm{BS}}}$ in Eq. (23) is zero.

Last, we express the derivative of $\mathcal{B}_{\sigma^2}(sT)$ as

$$\frac{\partial \mathcal{B}_{\sigma^2}(sT)}{\partial \lambda_{\mathrm{BS}}} = -T\sigma^2 e^{-sT\sigma^2} \frac{\partial f_s(r_{\mathrm{H}})}{\partial \lambda_{\mathrm{BS}}}, \tag{24}$$

where $\frac{\partial f_s(r_{\mathrm{H}})}{\partial \lambda_{\mathrm{BS}}}$ is given in Eq. (17).

The above modifications are necessary for the derivative w.r.t. λ_{BS}. However, for the derivative w.r.t. λ_{RIS}, no modification is needed. This is because adding RISs does not change the underlying spatial deployment of the BSs, and the expression in Eq. (16), modified by removing the integration over the distribution of r, gives the derivative for this scenario.

D. Incremental Investment Strategy

We now discuss how the above derivatives allow one to develop a strategic approach for incremental investment in deploying RIS-enhanced cellular systems. Recall that the RoI is assumed to be proportional to the ergodic rate, while the TCO is proportional to the number of deployed BSs and RISs. In each investment round, we use the partial derivatives $\frac{\partial \tau}{\partial \lambda_{\mathrm{BS}}}$ and $\frac{\partial \tau}{\partial \lambda_{\mathrm{RIS}}}$ to quantify the expected increase in ergodic rate, denoted by E, as a result of an increase in the density of either BS or RIS due to an investment. Therefore, we assume $E_{\mathrm{BS}} = \frac{\partial \tau}{\partial \lambda_{\mathrm{BS}}}$. However, note that the number of RIS in a given area depends not only on the RIS density but also on the number of BS and the size of the RIS cluster ring. As a result, we have $E_{\mathrm{RIS}} = \frac{1}{\lambda_{\mathrm{BS}}\mathcal{A}} \frac{\partial \tau}{\partial \lambda_{\mathrm{RIS}}}$, where $\mathcal{A}$ is the area of the cluster ring.

Here, the decision-making process is determined by comparing the expected gain ratio to the cost ratio to identify the more cost-effective investment. Recall that we define the cost ratio $J = \frac{\bar{C}_{\mathrm{BS}}}{\bar{C}_{\mathrm{RIS}}}$. With the investment costs for one round of BS or RIS deployment, $\Delta\bar{C}_{\mathrm{BS}}$ and $\Delta\bar{C}_{\mathrm{RIS}}$, defined in Eq. (3) and Eq. (4), the investment policy is given in Algorithm 1.

Algorithm 1 Policy for investment

Given the cost ratio $J = \frac{\bar{C}_{\mathrm{BS}}}{\bar{C}_{\mathrm{RIS}}}$ ▷ *Cost of Ownership*
while investing **do**
  Get $\lambda_{\mathrm{BS}}, \lambda_{\mathrm{RIS}}$
  Performance sensitivity to λ_{BS}: $E_{\mathrm{BS}} = \frac{\partial \tau}{\partial \lambda_{\mathrm{BS}}}$
  Performance sensitivity to λ_{RIS}: $E_{\mathrm{RIS}} = \frac{1}{\lambda_{\mathrm{BS}}\mathcal{A}} \frac{\partial \tau}{\partial \lambda_{\mathrm{RIS}}}$
  if $\frac{E_{\mathrm{BS}}}{E_{\mathrm{RIS}}} \geq J(1 + \lambda_{\mathrm{RIS}}\mathcal{A}/J)$ **then**
    Allocate the investment to increase the BS density
  else
    Allocate the investment to increase the RIS density

IV. Numerical Results and Decision Analysis

The system parameters for the numerical analysis[5] are as follows unless otherwise specified. Throughout the simulation, we consider a BS density ranging from 3 to 40 BS/km^2, resulting in average cell radii ranging from approximately 80 to 300 meters. The geometry of RIS clusters is fixed. It has an inner radius of 20 meters and an outer radius of 30 meters. Plot labels indicate the number of RIS elements of each RIS panel, representing varying beamforming capabilities. We consider that each BS transmits at $P_0 = 30$dBm, and the noise power is set as -100dBm.

A. Investment of RISs for Throughput Enhancement

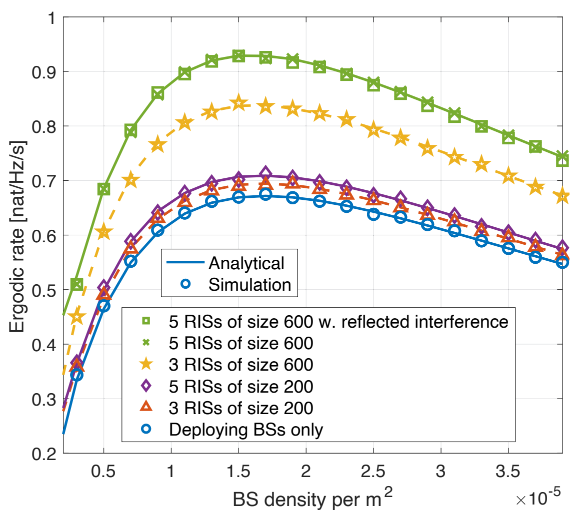

Fig. 3: Mean ergodic rate of a typical UE as a function of the density of BSs for different RIS densities and sizes

Fig. 3 depicts the ergodic rate of a typical UE as a function of the BS density[6], where the guard zone R_c is 50 meters[7]. It also illustrates the impact of varying RIS densities of each cluster by considering 3 or 5 RISs per cluster. From

[5]The numerical simulation code for this work is available on GitHub: https://github.com/Sun8Guden/RISassistedCellularFramework in the following path: /ResearchApplication/TechnoEconomic.

[6]The BS density under consideration spans a range where the inter-BS distance is significantly greater than the cluster radius, ensuring that the RISs are in proximity to their associated BSs.

[7]This guard distance ensures that the UE is not in the near field of either BS or RIS.

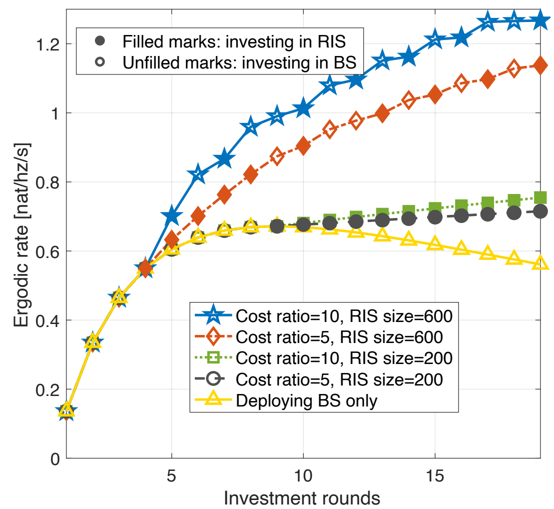

Fig. 4: Ergodic rate evolution based on investment in either BSs or RISs using Algorithm 1

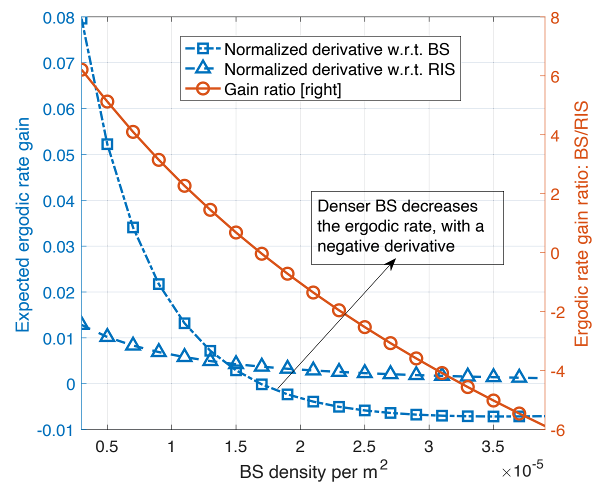

Fig. 5: Expected ergodic rate gains of single BS/RIS additions

Fig. 3, we observe that the mean ergodic rate is primarily constrained by the Gaussian noise when the BS density is low, and by the aggregated interference when the BS density becomes high. Note that the densification of BSs can be detrimental (in terms of spectral efficiency) above a certain BS density. This observation is consistent with the findings reported in [16]. Additionally, a higher BS density reduces the likelihood of a randomly located UE being outside the constant guard distance, reducing the probability of RIS-assisted communication. This also explains the decrease of the ergodic rate for a very high BS density. Furthermore, we simulate the scenario where all RISs reflect interference to other cells with a probability of beam overlapping 1% (for a beamwidth of 3.6 degrees[8]), depicted by green square marks in Fig. 3. By observing the overlap between the cross marks and square marks, we confirm that reflected interference is negligible when the overlap probability is low. Comparing the curves, we observe that the size of RIS is the most significant

[8]The half-power beamwidth for a 64-element RIS is estimated as 1-2 degrees in [17].

factor in improving the ergodic rate, with 600-element RIS significantly outperforming the 200-element one.

In Fig. 4, we discuss the successive deployment strategy for the throughput enhancement scenario based on Algorithm 1. The initial scenario assumes a deployment density of 1 BSs per km^2 without RISs. In each round, the operator has the investment budget that can deploy either 2 BSs per km^2 or equivalently $\bar{C}_{\mathrm{BS}}/\bar{C}_{\mathrm{RIS}}$ RISs. The investment is then directed toward deploying the type of node that yields a larger incremental gain. In particular, we assume cost ratios $\bar{C}_{\mathrm{BS}}/\bar{C}_{\mathrm{RIS}}$ to be 5 or 10, and consider the size of RIS to be either 200 or 600 elements[9]. In Fig. 4, filled marks indicate RIS investment, while unfilled marks denote BS investment. Fig. 4 demonstrates that a higher cost ratio not only results in an earlier decision to deploy RISs but also leads to a higher overall performance gain due to the ability to deploy more RISs with the same investment. Specifically, it is observed that the ergodic rate grows slowly when deploying small RISs (200 elements). However, RISs can still provide a solution for mitigating negative impacts in dense BS deployments. On the contrary, when RISs are larger (600 elements), they are capable of providing stronger reflected signals. The ergodic rate evolution suggests a preference for hybrid BS-RIS deployments.

Fig. 5 compares the expected ergodic rate gain from adding one BS or one RIS (600 elements) per km^2, based on the first-order derivatives of the mean ergodic rate w.r.t. the BS or RIS density[10]. This figure shows in the first place where the expected ergodic rate gain is positive and where it is negative. Note that both blue curves have a downward trend, suggesting a diminishing return on investment. A higher BS density means not only a stronger signal strength but also a higher interference power level. Indeed, an excessive investment allocation on BSs ultimately leads to negative returns [16]. In scenarios with high BS density, implying excessive interference, the investment in RIS emerges as the only solution, since the ergodic rate would degrade when deploying extra BSs, aligning with the investment decision in Fig. 4. Furthermore, the red curve represents the ratio of ergodic rate gains between deploying BSs or RISs. This characterizes the technological gain ratio between investing in an additional BS or RIS. An informed economic decision is made by comparing this ratio with the cost ratio coefficient. For example, in a scenario with BS density of 10^{-5}/m^2, it is more cost-effective to invest in RISs when the cost ratio exceeds 3, implying that deploying three RISs offers a better performance improvement than a BS with a lower TCO.

B. Investment of RISs for Coverage Hole Mitigation

Recall that C_{H} scales this distance in Eq. (1). To ensure the RIS cluster is deployed mostly within the cell, we select C_{H} such that the average distance from the coverage hole to the BS is 80 meters[11] when $\lambda_{\mathrm{BS}} = 10^{-5}/\mathrm{m}^2$. We will focus on examining how the direct link blockage penalty influences the deployment strategy. Recall that the expected ergodic rate gain ratio (Fig. 5) is introduced to assess technological preference compared with economic cost. We plot this ratio for the coverage hole scenario to provide insights into deployment decisions, which in turn lead to an investment policy.

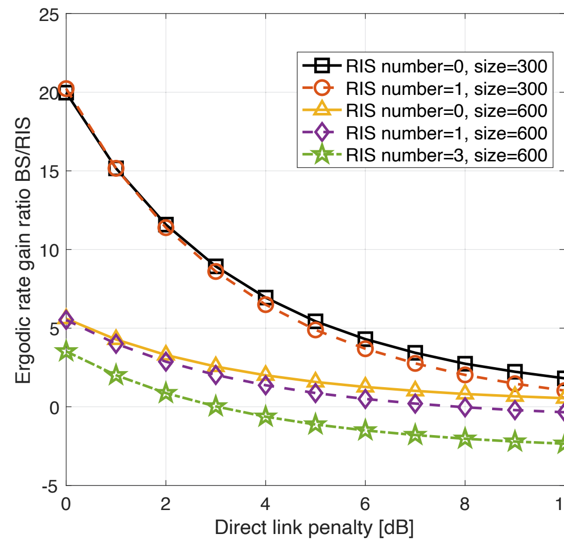

Fig. 6: Expected ergodic rate gain ratio between adding new BS or RIS as a function of direct link penalty

Fig. 6 shows the expected gain ratio as a function of the direct link penalty K, which takes values from 0 to 10 dB. We consider the parameters including the size of RISs and the number of existing RISs in each cell. In general, these curves in Fig. 6 decrease, suggesting that, when the direct link to the UE in the coverage hole is severely degraded, the preference for the deployment of BS over RIS decreases. Fig. 6 shows that a moderate cost ratio (e.g., 5) could favor deploying large RISs (600 elements), but may not incentivize deploying small RISs (300 elements) unless the direct link is severely penalized. As observed in the curves marked with circles, diamonds, and stars, when BSs are already equipped with a certain number of RISs per cluster, increasing the BS density becomes less favorable since it implies the cost of adding new RISs in the area. In the specific case where each BS is configured with an average of three RISs, as shown by the curve marked by green stars, deploying a new BS equipped with three RISs may be less advantageous than allocating these three RISs to existing BSs, given that the expected gain ratio is mostly negative.

The successive investment plan is plotted in Fig. 7. The scenario starts with a BS density of $5/\mathrm{km}^2$ without any RISs. In each investment round, one can either deploy one BS or several RISs according to the cost ratio $\bar{C}_{\mathrm{BS}}/\bar{C}_{\mathrm{RIS}}$. As in Fig. 4, filled marks indicate RIS investment, and unfilled marks denote BS investment in each round. Without considering blockage, the performance improvement due to RIS is compared with the

[9]The authors in [18] confirm a cost ratio of approximately 5 between a BS and a RIS.

[10]Note that the RIS density derivative is defined per cluster. To enable a fair comparison between the impact of adding one RIS or one BS per km^2, we scaled the derivatives accordingly.

[11]For two-dimensional PPP-modeled cellular networks, the average distance between any point and its nearest BS is $1/(2\sqrt{\lambda_{\mathrm{BS}}})$, approximately 150 meters for $\lambda_{\mathrm{BS}} = 10^{-5}/\mathrm{m}^2$.

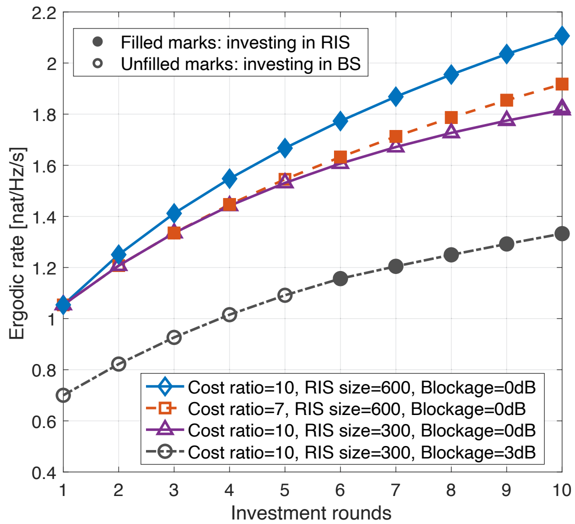

Fig. 7: Ergodic rate evolution for coverage hole mitigation scenario based on investment in either BSs or RISs

purple curve marked with triangles, which solely invests in BSs. This is because deploying 300 elements RIS cannot outperform adding BSs with the same investment. Different branches emerge for varying cost ratios and investment decisions when the RIS is equipped with a significant number of elements for beamforming (600 elements). When the cost ratio is 7, as depicted by the curve with square marks, the optimal strategy involves alternating investments between BSs and RISs, resulting in a modest performance enhancement. When RISs are both large (600 elements) and cost-efficient ($\bar{C}_{\rm BS}/\bar{C}_{\rm RIS} = 10$), deploying RIS is always preferable, as shown by the blue curve marked with diamonds. Moreover, Fig. 7 also shows that the blockage significantly influences the ergodic rate and the investment policy. The black curve with circle marks, representing a 3dB penalty, is distinctly separated from the other curves that have no penalty. Notably, with the 3dB penalty, investment shifts to RIS when the BS density exceeds a certain threshold, while without penalty (triangle marks) investment remains in BSs.

V. Conclusion

A well-designed RIS deployment strategy is key to successful cellular network densification. We proposed a first techno-economic analysis for optimizing investments by modeling the RIS-assisted cellular network using stochastic geometry and considering the relative costs of deploying BSs and RISs. A sensitivity analysis is conducted to assess the impact of parameter changes, including the density of BSs and RIS, and their unit cost, on the system's ergodic rate for both throughput enhancement and coverage hole mitigation scenarios. Analytical expressions are derived to devise an optimal deployment strategy based on techno-economic considerations. Numerical results illustrate how investment decisions, determined by cellular network conditions, impact the evolution of ergodic rates for both scenarios. This work provides quantitative insights into techno-economic factors for network operators to maximize RoI when deploying RIS-assisted cellular networks.

Acknowledgement

The work of F. Baccelli and G. Sun was supported by the European Research Council project titled NEMO under grant ERC 788851. The work of F. Baccelli was also supported by the French National Agency for Research project titled France 2030 PEPR réseaux du Futur under grant ANR-22-PEFT-0010.

References

[1] D. Xu, A. Zhou, X. Zhang, G. Wang, X. Liu, C. An, Y. Shi, L. Liu, and H. Ma, "Understanding Operational 5G: A First Measurement Study on its Coverage, Performance and Energy Consumption," in *Proceedings of the Annual conference of the ACM Special Interest Group on Data Communication on the Applications, Technologies, Architectures, and Protocols for Computer Communication*, pp. 479–494, 2020.

[2] R. Liu, Q. Wu, M. Di Renzo, and Y. Yuan, "A Path to Smart Radio Environments: An Industrial Viewpoint on Reconfigurable Intelligent Surfaces," *IEEE Wireless Communications*, vol. 29, no. 1, pp. 202–208, 2022.

[3] J. Wang, Y.-C. Liang, J. Joung, X. Yuan, and X. Wang, "Joint Beamforming and Reconfigurable Intelligent Surface Design for Two-Way Relay Networks," *IEEE Transactions on Communications*, vol. 69, no. 8, pp. 5620–5633, 2021.

[4] E. Lang, S. Redana, and B. Raaf, "Business Impact of Relay Deployment for Coverage Extension in 3GPP LTE-Advanced," in *2009 IEEE international conference on communications workshops*, pp. 1–5, IEEE, 2009.

[5] F. Baccelli, B. Błaszczyszyn, *et al.*, "Stochastic Geometry and Wireless Networks: Volume II Applications," *Foundations and Trends® in Networking*, vol. 4, no. 1–2, pp. 1–312, 2010.

[6] J. Lyu and R. Zhang, "Hybrid Active/Passive Wireless Network Aided by Intelligent Reflecting Surface: System Modeling and Performance Analysis," *IEEE Transactions on Wireless Communications*, vol. 20, no. 11, pp. 7196–7212, 2021.

[7] G. Sun, F. Baccelli, K. Feng, L. U. Garcia, and S. Paris, "A Stochastic Geometry Framework for Performance Analysis of RIS-assisted OFDM Cellular Networks," *arXiv preprint arXiv:2310.06754*, 2023.

[8] J. G. Andrews, F. Baccelli, and R. K. Ganti, "A Tractable Approach to Coverage and Rate in Cellular Networks," *IEEE Transactions on communications*, vol. 59, no. 11, pp. 3122–3134, 2011.

[9] F. Baccelli, B. Błaszczyszyn, and M. Karray, "Random Measures, Point Processes, and Stochastic Geometry," 2020.

[10] S. N. Chiu, D. Stoyan, W. S. Kendall, and J. Mecke, *Stochastic Geometry and its Applications*. John Wiley & Sons, 2013.

[11] Q. Wu and R. Zhang, "Intelligent Reflecting Surface Enhanced Wireless Network via Joint Active and Passive Beamforming," *IEEE Transactions on Wireless Communications*, vol. 18, no. 11, pp. 5394–5409, 2019.

[12] S. Zeng, H. Zhang, B. Di, Y. Tan, Z. Han, H. V. Poor, and L. Song, "Reconfigurable Intelligent Surfaces in 6G: Reflective, Transmissive, or Both?," *IEEE Communications Letters*, vol. 25, no. 6, pp. 2063–2067, 2021.

[13] J. Wang, Y.-C. Liang, Y. Pei, and X. Shen, "Reconfigurable Intelligent Surface as a Micro Base Station: A Novel Paradigm for Small Cell Networks," *IEEE Transactions on Wireless Communications*, vol. 22, no. 4, pp. 2338–2351, 2022.

[14] V. I. Bogachev and M. A. S. Ruas, *Measure Theory*, vol. 1. Springer, 2007.

[15] G. Sun, F. Baccelli, L. U. Garcia, and S. Paris, "A Stochastic Geometry Based Techno-Economic Analysis of RIS-Assisted Cellular Networks," *arXiv preprint arXiv:2501.12037*, 2025.

[16] A. AlAmmouri, J. G. Andrews, and F. Baccelli, "SINR and Throughput of Dense Cellular Networks with Stretched Exponential Path Loss," *IEEE Transactions on Wireless Communications*, vol. 17, no. 2, pp. 1147–1160, 2017.

[17] H. Han, Y. Liu, and L. Zhang, "On Half-power Beamwidth of Intelligent Reflecting Surface," *IEEE Communications Letters*, vol. 25, no. 4, pp. 1333–1337, 2020.

[18] M. Rossanese, A. Garcia-Saavedra, A. E. Lutu, and X. Costa Perez, "Data-Driven Analysis of the Cost-Performance Trade-off of Reconfigurable Intelligent Surfaces in a Production Network," *Proceedings of the ACM on Networking*, vol. 1, no. CoNEXT3, pp. 1–20, 2023.